Estimates of net heat fluxes over the Atlantic Ocean

R. T. Pinker,[1] A. Bentamy,[2] K. B. Katsaros,[3,4] Y. Ma,[1] and C. Li[1]

Received 29 August 2013; revised 16 December 2013; accepted 19 December 2013; published 21 January 2014.

[1] Many studies have been undertaken to evaluate turbulent heat fluxes at the ocean-atmosphere interface; less was done on the total *net heat flux*. We will compare heat budgets at the ocean-atmosphere interface as derived from satellites and from blended products, compare them to in situ observations, identify the location of largest differences, and attempt to explain reasons for these differences. The results over the Atlantic Sector (50°S–50°N) for a 3 year period show that differences in the turbulent fluxes among two widely used approaches are overshadowed by differences in the radiative fluxes. While the maximum difference in sensible and latent heat fluxes can be about 30 W/m^2, the mean values for latent heat fluxes are −2.27 W/m^2 for January and 5.40 W/m^2 for July. For sensible heat, they are 2.82 W/m^2 for January and 5.64 W/m^2 for July. We show that the maximum difference in net radiative fluxes can be as high as 55 W/m^2, for January, the mean difference in net SW is 6.31 W/m^2 and in net LW it is 12.14 W/m^2. For July, the respective differences are −9.99 W/m^2 for the SW and 14.31 W/m^2 for the LW. Relationships between the fluxes and satellite derived surface wind speed, total precipitable water, and cloud cover provide insight on the dominant processes that control the net heat flux. This study is intended to present an estimate of uncertainties that still exist in the net heat flux at the ocean-atmosphere interface.

Citation: Pinker, R. T., A. Bentamy, K. B. Katsaros, Y. Ma, and C. Li (2014), Estimates of net heat fluxes over the Atlantic Ocean, *J. Geophys. Res. Oceans*, *119*, 410–427, doi:10.1002/2013JC009386.

1. Background

[2] The Atlantic sector shows climatic variability on a wide range of spatial and temporal scales [*Hastenrath*, 1984; *Ruiz-Barradas et al*., 2000; *Kushnir et al*., 2006; *Hurrell and Deser*, 2009; *Hu et al*., 2011]. The tropical Atlantic is also the genesis region of most hurricanes reaching the North American continent [*Emanuel*, 1988; *Landsea et al*., 2012]. Interest in the region is also motivated by the extended droughts in West Africa and the search for its explanation. The net heat flux at the ocean-atmosphere interface is believed to play an important role in these interactions and therefore, it is of interest to establish how well such fluxes can be estimated. For instance, the importance of Atlantic SST variations and onshore moisture flux for the drought-ridden Sahel region was demonstrated by *Liu et al*. [2012]. Recommendations and priorities for research in the Atlantic are outlined in the U.S.-CLIVAR Atlantic implementation plan (http://www.usclivar.org/plans.php). The need to improve estimates of air-sea fluxes and atmospheric reanalysis products, which are widely used to study climatic change in the ocean and the atmosphere, are among top priorities.

[3] Comparison of turbulent air-sea flux estimates from various models [e.g., *Smith et al*., 2010; *Bourassa et al*., 2013] reveals large differences between the estimates. Yet, it is the net surface flux (including radiative flux) that is of interest. For instance, it was shown by *Shinoda et al*. [1998] that for the southwestern tropical Indian Ocean seasonal variations of mixed layer heat content are driven by a combination of the *net surface heat flux*, horizontal heat advection, and vertical turbulent mixing at the base of the mixed layer. *Foltz et al*. [2003] discuss the seasonal mixed layer heat budget of the tropical Atlantic Ocean. They have also shown that the *net surface heat flux* varies in phase with the mixed layer heat storage rate and depends very much on the *surface shortwave* (SW) radiation. As such, estimating the relative magnitudes of the various fluxes and existing differences is of interest.

[4] Shortwave fluxes are dominated by clouds and atmospheric constituents; the most unknown ones are aerosols. The impact of extreme aerosol loading such as volcanic eruptions has been discussed in numerous early studies; it was shown that for several years global mean sea surface temperature (SST) and ocean heat content can be lowered by −0.3 to −0.5°K relative to longer term temperature trends [*Angell and Korshover*, 1985; *Angell*,

[1]Department of Atmospheric and Oceanic Science, University of Maryland, College Park, Maryland, USA.
[2]Institut Francais de Recherche pour l'Exploitation de la Mer, Plouzane, France.
[3]Rosenstiel School of Marine and Atmospheric Science, University of Miami, Miami, Florida, USA.
[4]Northwest Research Associates Inc., Redmond, Washington, USA.

Corresponding author: R. T. Pinker, Department of Atmospheric and Oceanic Science, University of Maryland, Space Sciences Bldg., College Park, MD 20742, USA. (pinker@atmos.umd.edu)

2169-9275/14/10.1002/2013JC009386

1988]. Models have shown that the cooler water is primarily affecting the upper 1000 m where it persists for many decades [*Gleckler et al*., 2006; *Driscoll et al*., 2012]. *Otterå et al*. [2010] discuss model results that show that major eruptions strengthen the North Atlantic Ocean meridional overturning circulation (AMOC) by a Sverdrup (1×10^6 m^{-3} s^{-1}) or more over a 5–15 year time scales which corresponds to a significant 5% increase in the Atlantic's contribution to the earth's meridional heat transport. Therefore, improved estimates of SW radiation that reaches the ocean surface and that accounts for the effect of aerosols is of significance.

[5] Using two well-established methodologies based on multiple satellite sensors and numerical analyses, an attempt is being made here to obtain all the heat flux components (latent, sensible, and radiative) at the ocean surface over the Atlantic Ocean, to better understand where and why differences occur. The fluxes are generated at daily and monthly time scales between 50°N and 50°S for a 3 year period at 1° resolution (some parameters were derived at higher resolutions). The turbulent fluxes are based on those developed at the Institut Francais de Recherche pour l'Exploitation de la Mer (IFREMER) [*Bentamy et al*., 2013] and at the Woods Hole Oceanographic Institution's Objectively Analyzed air-sea Fluxes (WHOI OAFlux) [*Yu et al*., 2008] (see Table 1).

[6] Methodologies to derive radiative fluxes from long-term satellite observations are described, for example, in *Zhang et al*. [2004] and *Ma and Pinker* [2012], methods that use more recent satellite observations (as also used in this study) are described in *Wang and Pinker* [2009] and *Nussbaumer and Pinker* [2012]. The methodologies how the various fluxes were computed will be summarized in section 2. Data used will be reviewed in section 3. In section 4, we discuss findings on radiative fluxes, net total fluxes (radiative and turbulent) followed by analysis of time series of the flux components and the variables that control them for selected latitude and longitude locations. Summary and conclusions are given in section 5.

2. Turbulent Heat Fluxes and Their Evaluation

2.1. IFREMER Heat Flux Estimation Methodology

[7] In this study, we use an updated version of the IFREMER turbulent flux estimates [*Bentamy et al*., 2013] as available at daily time scale over global oceans at a spatial resolution of 0.25° in longitude and latitude. Compared to previous estimates [*Bentamy et al*., 2008], numerous improvements have been incorporated in terms of methodology and auxiliary data.

[8] The formulas used are the bulk transfer relations for latent (LH) and sensible heat flux (SH) given as:

$$LH = -L\rho C_E W_{10}(Q_{a10} - Q_s) \quad (1)$$

$$SH = -C_p \rho C_H W_{10}(T_{a10} - T_s) \quad (2)$$

$$T* = LH + SH \quad (3)$$

where, W_{10}, Q_{a10}, and T_{a10} are the surface wind speed, specific air humidity, and air temperature at 10 m height; Qs is the saturation specific humidity at the sea surface temperature (SST) denoted as Ts; L (2.45×10^6 J/kg) is the latent heat of evaporation coefficient; $C_p = 1005$ J/kg is the specific heat of air at constant pressure; ρ is the air density. The bulk transfer coefficients for latent heat flux (C_E, Dalton number), and sensible heat flux (C_H, Stanton number) are estimated from wind speed, air temperature, and SST using the COARE3.0 parameterization [*Fairall et al*., 2003].

[9] The bulk variables such as surface wind speed (W_{10}) and specific air humidity (Q_{a10}) at 10 m height are estimated from remotely sensed observations. W_{10} is obtained from the SeaWind scatterometer on board QuikSCAT satellite as available from the Jet Propulsion Laboratory (JPL, 2006) (see Table 1). A previous model [*Bentamy et al*., 2003] is enhanced to retrieve Q_{a10} from the special microwave imager (SSM/I) sensor brightness temperatures (T_b) measurements. The new satellite estimates of Q_{a10} are used in combination with the newly reprocessed QuikSCAT *V3* (ftp://podaac.jpl.nasa.gov/OceanWinds/quikscat/preview/L2B12/v3/), the latest version of sea surface temperature (SST) analyses provided by the National Climatic Data Center (NCDC), and with 10 m air temperature estimated from the European Centre for Medium Range Weather Forecasts (ECMWF) reanalyses (ERA Interim) [*Simmons et al*., 2006], to determine daily gridded surface wind stress, latent (LH), and sensible (SH) heat fluxes, at a spatial grid resolution of 0.25°.

2.2. Quality Assessment of IFREMER Heat Fluxes

[10] For this study, the quality of the new daily averaged turbulent fluxes is assessed by comparison with daily fluxes estimated from meteorological bulk variables measured at moored buoys in the Atlantic Ocean. The latter include Atlantic moorings off the French and England coasts maintained by UK Met-Office and/or Météo-France (MFUK), moorings off the Atlantic U.S. coasts maintained by the National Data Buoy Center (NDBC), and moorings from the Prediction and Research Moored Array in the Atlantic (PIRATA) network in the equatorial Atlantic. All in situ values are hourly averages. Measurement height varies between 3 and 10 m depending on mooring configuration. Buoy wind, specific air humidity, and air temperature are converted to the standard height of 10 m using the COARE3.0 algorithm of *Fairall et al*. [2003]. Similar validation procedure has been used in *Bentamy et al*. [2013] but limited to the period 2003–2005. Here, the validation of daily satellite fluxes is extended to the period October 1999 to November 2009. Overall, the LH biases (buoy minus satellite) from the MFUK, NDBC, and tropical moorings are 1 W/m^2, 9 W/m^2, and 3 W/m^2, respectively. The respective SH biases are −1, −1, and −4 W/m^2. Daily satellite LH (SH) fluxes are slightly underestimated (overestimated) as compared to buoy estimates. The associated standard deviation (STD) differences do not exceed 30 W/m^2 for MFUK and tropical comparison, whereas for NDBC, STD reaches 59 W/m^2. The latter result is mainly due to the discrepancy between buoy and satellite specific air humidity. One should note that most NDBC buoys do not provide measurement of specific air humidity or of relative humidity. We estimate specific humidity from air and dew point temperatures. To further assess the comparison between buoy and satellite fluxes, bias, STD, and correlation values are estimated from collocated data at each buoy

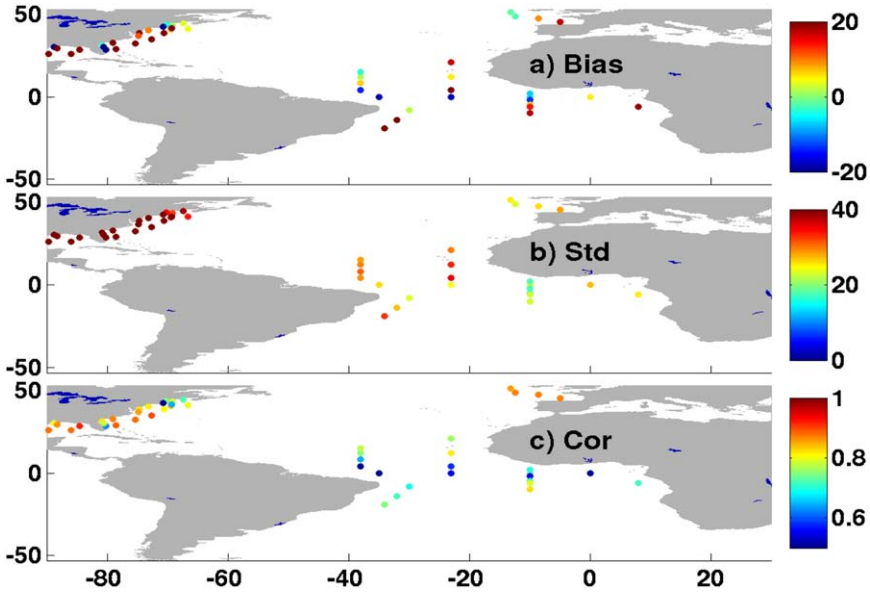

Figure 1. Statistical parameters characterizing difference between daily averaged buoy and daily analyses of satellite latent heat flux estimates as derived by *Bentamy et al*. [2013]: (a) bias, (b) standard deviation, and (c) correlation values at each buoy location. Statistics are calculated for the period 1999–2009.

location. Figure 1 illustrates results for LH fluxes while Figure 2 shows results for SH fluxes. Except at NDBC locations, most of LH biases are lower than 15 W/m^2 and the related STD are lower than 30 W/m^2. The main significant difference pattern is found along the equatorial region. Satellite LH tends to be overestimated compared to buoy estimates. The results from the satellite retrievals in low wind conditions characterizing the equatorial area (Figure 2) indicate improvement compared to previous comparison results [*Santorelli et al*., 2011] based on the earlier version of IFREMER estimates [*Bentamy et al*., 2008]. Most of the bias and the STD values do not exceed 10 and 20 W/m^2, respectively. Yet, the satellite estimates of daily SH flux tend to be slightly overestimated compared to observations due to underestimation of 10 m air temperature in ERA Interim compared to buoy data (used to calculate satellite SH) [*Bentamy et al*., 2013]. The most pronounced SH flux differences are found along the Atlantic north-western regions, the locations of the highest SH values [*Bentamy et al*., 2013]. Buoys and satellites exhibit high correlation (>0.85) at MFUK and NDBC locations, whereas at PIRATA locations, the correlation coefficients do not exceed 0.72 due to the use of daily averaged air temperatures from ERA Interim which shows poor agreement with daily PIRATA buoy data [*Bentamy et al*., 2013]. An example of the frequency distribution of the turbulent heat fluxes as derived from the IFREMER product is illustrated in Figure 3. The statistical analysis in this figure and those to follow was conducted over a region of the Atlantic Oceanic basin between 50°S and 50°N. They are shown for January and for July months of 2003–2005. The main peak observed in LH during winter is mostly associated with evaporation occurring along the trade wind areas. The secondary LH peak around 150 W/m^2 is mainly due to strong LH loss drawing from the warm Gulf Stream off the east coast of the U.S. In these regions, the LH experiences the strongest annual variation peaking during the winter, when cold dry continental air off-shore of North America crosses the Gulf Stream north wall in the Atlantic [*Grodsky et al*., 2009]. Sensible heat flux distributions (Figures 3b and 3d) indicate that SH values are 5 times lower than LH values. The mean SH values are dominated by observations occurring in tropical and extratropical areas. Values exceeding 40 W/m^2 are mainly found around 40°N in the Atlantic Ocean during the winter season as a result of a combination of high winds and high difference between sea surface and air temperatures (ΔT). Due to the seasonal variability of surface wind and (ΔT), the depicted SH flux local maxima vanish in summer time. Based on results from satellite flux comparisons to buoy observations the new IFREMER approach was selected as a prototype for satellite estimation methodology.

2.3. WHOI OAFlux Flux Products

[11] A different approach was taken by the group at the Woods Hole Oceanographic Institution (WHOI) who use optimal interpolation of information from satellite data (SSM/I) and models (ECMWF and NCEP2) such as wind speed, air temperature (model only), humidity, and SST to produce daily bulk turbulent flux fields over global Oceans with a spatial resolution of 1° in longitude and latitude [*Yu et al*., 2008]. These heat fluxes are available for years 1985–2013 and are referenced as Objectively Analyzed Air-sea Fluxes (OAFlux). The WHOI product was selected as a representative of model dependent category and for its demonstrated high quality as also shown in *Santorelli et al*. [2011] who compared the *Bentamy et al*. [2008] IFREMER and OAFLux turbulent fluxes over the Atlantic Ocean. Since the turbulent fluxes of the OAFlux product used in this study have been evaluated previously, the reader is referred to *Santorelli et al*. [2011] for details.

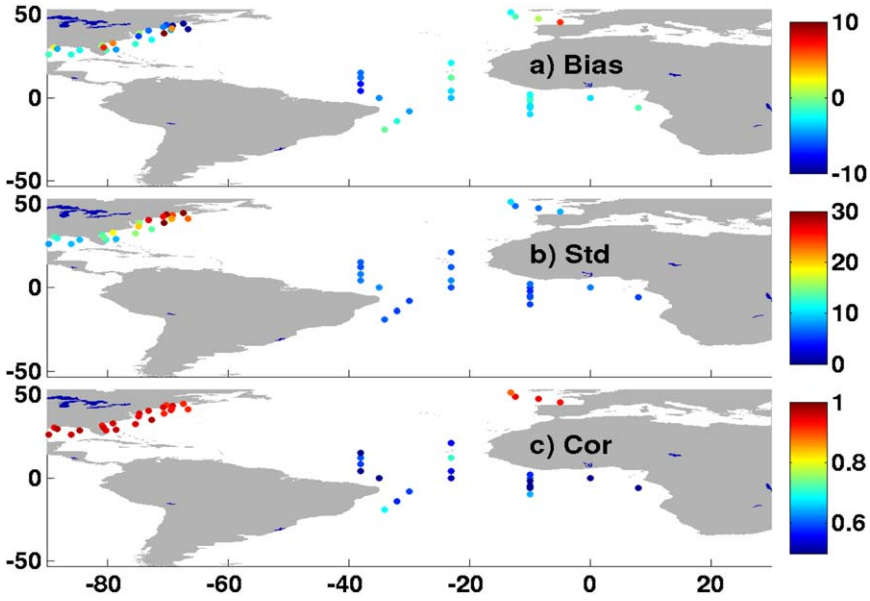

Figure 2. As Figure 1 for sensible heat fluxes.

2.4. Differences Between IFREMER and OAFlux Products

[12] This section aims to highlight the agreement and the main differences between the latent and sensible heat fluxes derived from IFREMER and from OAFLux. The former are expected to have significant impact on the comparisons of net heat fluxes (section 4). One should note that neither product is considered as reference. The comparisons between IFREMER and OAFLux LH and SH are investigated through the spatial distributions of the mean difference, the associated standard deviation, and the correlation coefficients estimated at each grid point. Both products exhibit similar spatial structures of LH and of SH for winter as well as for summer seasons (not shown). The correlation coefficient values are about higher than 0.90 over regions located north and south of 10°N and 10°S, respectively. The lowest correlations are found in the equatorial region, mainly related to low wind speed variability. The features of IFREMER and of OAFlux LH and SH exhibit the main known flux spatial patterns [e.g., *Bentamy et al*., 2013]. For instance, the two products indicate that the largest LH and SH values occur during the winter season over the western boundary region with means exceeding 250 W/m^2 and 150 W/m^2, respectively. The minima are mainly found along the eastern boundaries, mostly related to the oceanic advection of cold water (along with some upwelling as found off the North and South African coasts during winter and summer, respectively). Mean latent and sensible heat flux differences between IFREMER and OAFlux products are illustrated in Figure 4. They are estimated for January and July of 2003, 2004, and 2005. Figures 4a (January) and 4c (July) show the spatial patterns of latent heat flux differences, while Figures 4b and 4d show the sensible heat flux differences. On average, the mean differences are lower than 30 and 10 W/m^2 for latent and sensible heat fluxes, respectively. These results show closer agreement between the two products than previous results based on

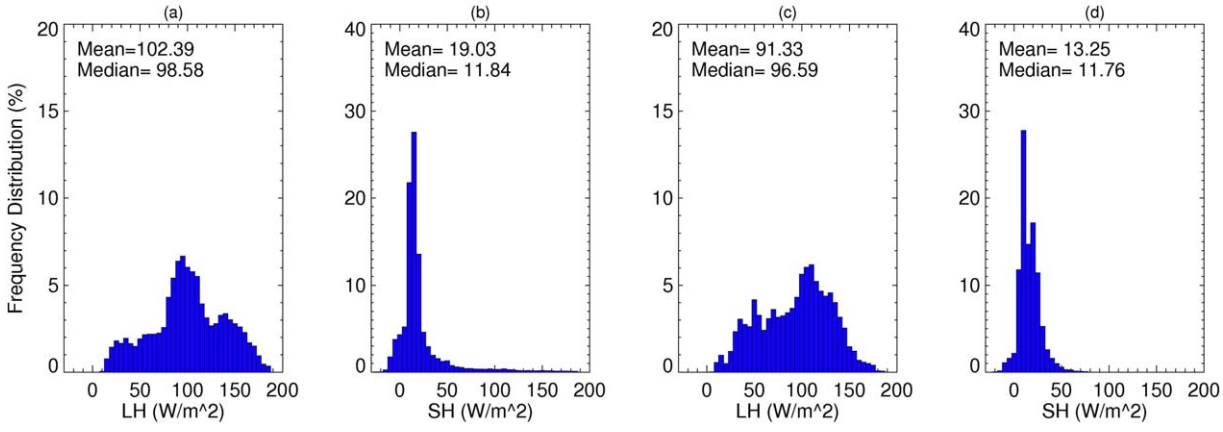

Figure 3. Histograms of mean values of: (a) latent and (b) sensible heat fluxes for January and (c) latent and (d) sensible heat fluxes for July as available from IFREMER [*Bentamy et al*., 2013] for 2003–2005.

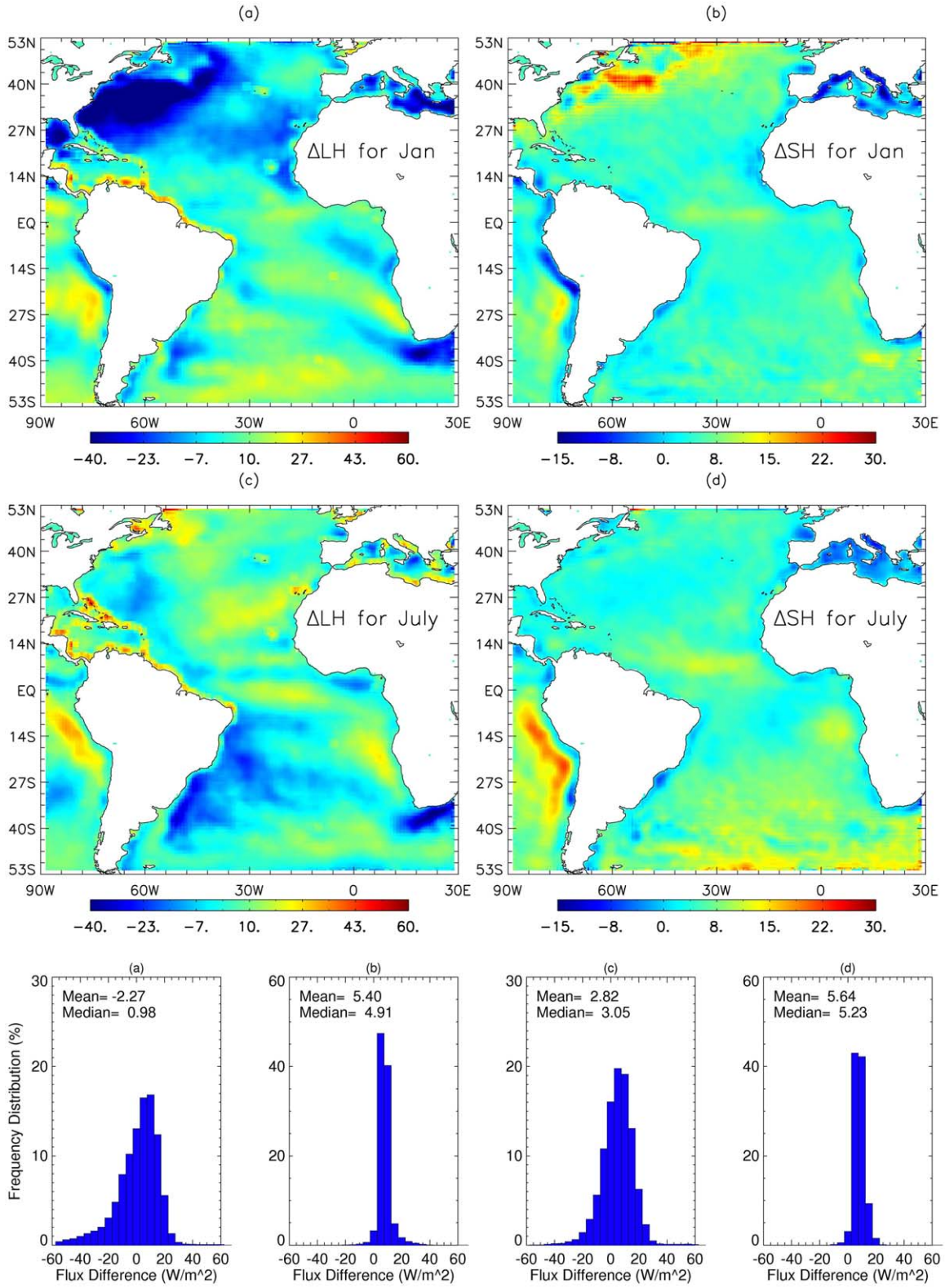

Figure 4. (top) Differences in (a) latent and (b) sensible heat fluxes for January and (c) latent and (d) sensible heat fluxes for July as available from IFREMER [*Bentamy et al*., 2013] and WHOI OAFlux [*Yu et al*., 2007] for 2003–2005. (bottom) Histogram of differences for above.

IFREMER data from *Bentamy et al*. [2008] as reported in *Santorelli et al*. [2011]. The reduction in the differences between IFREMER and WHOI fluxes is clearly seen in the tropical area. For instance, latent heat flux difference are within 20 W/m^2, whereas previously [*Santorelli et al*., 2011] the discrepancies exceeded 40 W/m^2.

[13] The largest discrepancies between IFREMER and OAFlux (in this order) exceeding 30 W/m^2 are found off the East Coasts of the Northern Atlantic Ocean (Figure 4a) along the Gulf Stream region. Conditions in this region present challenges in satellite flux estimation, including strong surface currents and SST gradients as well as how the stratified atmospheric boundary layer amplifies air-sea interactions on an intraseasonal timescale [*Grodsky et al*., 2009]. The depicted differences between IFREMER and OAFlux LH are associated with discrepancies in both specific air humidity (Q_a) and wind speed (W_{10}). IFREMER Q_a tends to be higher than OAFlux Q_a, whereas IFREMER W_{10} is lower than OAFlux W_{10}. Mean differences of Q_a reach and may exceed at some locations 1 g/kg, while differences in W_{10} are about -1 m/s. Differences in W_{10} may be addressed by using NDBC buoy daily wind averages. The mean difference, estimated for January of 2003–2005, between daily wind speeds derived from IFREMER product and from buoys moored off US western coats (WMO 44008 and WMO 44011) is about 0.45 m/s, leading to a slight overestimation of IFREMER wind speed. This is in opposite direction for explaining the result above for IFREMER and OAFlux comparisons. Unfortunately, NDBC specific air humidities are not available, which would allow to assess IFREMER and OAFlux Q_a differences. The comparison of sensible heat fluxes (Figures 4b and 4d) indicates quite a small bias between the two products. It is somewhat lower than 5 W/m^2. The largest departures are found over the western boundary currents and over southern extratropical regions for January and July, respectively. IFREMER SH fluxes tend to be slightly higher than OAFlux over most of the Atlantic areas. This is mainly related to differences in sea surface and air temperature used in the estimation of each SH in the two products.

[14] Over the Atlantic sector (70°W–30°E, 45°S–45°N) the variables that enter the bulk formulae for computing fluxes (wind speed, sea surface and air temperature, and specific humidity) can be evaluated against buoys in the Prediction and Research Moored Array in the Atlantic (PIRATA). Detailed evaluation was performed earlier by *Santorelli et al*. [2009] for the period 1996–2005. Since WHOI assimilates PIRATA observations, the evaluation was done against independent buoy data from two University of Miami deployments ASIS (Air-Sea Interaction Spar) buoys [*Graber et al*., 2000]; FETCH [*Hauser et* al., 2003]; and ROMEO [*Zhang et al*., 2009]. To examine how each variable contributes to the difference between estimated and buoy fluxes, the method of *Bourras* [2006] was applied which showed that specific air humidity and air temperature contributed the most to the biases of IFREMER latent and sensible heat fluxes, respectively, at both independent buoys. For WHOI OAFlux products, deviations from FETCH values were mainly due to wind speed and sea surface temperature differences, while in comparison with ROMEO fluxes, WHOI OAFlux biases were primarily due to specific humidity and sea surface temperature estimates. Modified estimates of turbulent fluxes with the IFREMER approach using the 10 m specific humidity and air temperature products of *Jackson et al*. [2009] have shown significant improvements. Differences are also depicted in the South African oceanic area. Strong storm systems that propagate over the Agulhas Current region off the South African coast produce strong latent heat flux; depending on the location of the storm center, this heat flux is sometimes amplified by anomalous southerly winds that bring dry and cold sub-Antarctic air northward [*Grodsky et al*., 2009]. The satellite observations may be unable to handle this phenomenon properly, which could cause a discrepancy between IFREMER and WHOI OAFlux products in this region. Model fluxes may also suffer in areas where there is little in situ data to assimilate into the WHOI OAFlux product.

[15] The fact that IFREMER used the *Reynolds et al*. [2007] product that included AMSR-E data merged with AVHRR data from 2002 on compared to WHOI's use of the AVHRR only data may have been part of the reason for larger discrepancies in SST estimates used in the two products. Additional possible sources for differences can be related to humidity data from radiosondes used in numerical models and assimilated in the WHOI product. They are known to exhibit dry and wet biases, which depend on the radiosondes' type and age as well as the conditions of the environment [*Wang et al*., 2002]. *Bock et al*. [2007] showed that, for measurements of precipitable water vapor (PWV), which can be used to estimate humidity, over Africa (35°N–10°S), there were dry biases of 12–14% in radiosonde data compared to Global Positioning System (GPS) data, which partially explain biases of up to 9% for ERA-40 PWV data and up to 14% for NCEP2 PWV data.

3. Radiative Fluxes

3.1. Terminology

[16] The earth climate is a result of the balance maintained between the *solar radiation* absorbed by the atmosphere/earth system (gain) and the *emission* of the *terrestrial* radiation back to space (loss). This balance is also referred to as *net radiation* (Q^*) or *radiation balance* composed of *net solar* radiation and *net longwave* radiation expressed commonly as:

$$Q* = SW\downarrow - SW\uparrow + LW\downarrow - LW\uparrow \quad (4)$$

where SW (0.3–4.0 μm) and LW (4.0–100.0 μm) are the shortwave and longwave components, respectively, arrows represent the direction of the flux, and Q^* is the surface net radiation (0.3–100.0 μm). The net shortwave radiation is a balance between the incoming shortwave and the reflected shortwave; the ratio of reflected to incoming radiation is also known as the *albedo*.

$$K* = SW\downarrow(1 - \mathbf{a}) \quad (5)$$

[17] K^* is the surface net shortwave radiation (0.3–4.0 μm), and **a** is the albedo of the surface.

[18] To compute K^*, information on surface albedo (**a**) is needed. In principle, surface albedo can be supplied to the inference scheme from independent sources. The net longwave radiation is a balance between the incoming longwave and outgoing longwave given as:

$$L* = (LW\downarrow - LW\uparrow) \quad (6)$$

[19] L^* is the net longwave radiation at the surface (4.0–100.0 μm), and LW↑ depends on *surface temperatur*e and *emissivity* and can be determined as:

$$LW\uparrow = \varepsilon\sigma T_s^4 \quad (7)$$

where ε is surface emissivity, σ is the Stefan Boltzmann constant, and Ts is the sea surface temperature (SST).

[20] Absorption of solar radiation in the atmosphere is mostly by ozone, water vapor, carbon dioxide, oxygen, and clouds. Clouds play a major role in determining the net radiative balance via their optical properties and amount. The effect of clouds on the Earth's radiation balance is measured as the difference between the clear-sky and total-scene radiation results. This difference is defined as *cloud-radiative forcing*. *Cloud optical depth* is a general measure of the capacity of a cloud to control the amount of light that will reach the surface.

[21] Although the estimation of radiative fluxes from numerical weather prediction (NWP) models has improved during the last decade, accurate estimates are still lacking since cloud schemes are often problematic, especially when relatively high temporal and spatial resolution is desired (days and 50–100 km scales) [*Intergovernmental Panel on Climate Change* (*IPCC*), 2007]. Satellites (geostationary and polar-orbiting) provide global coverage and routine sampling and can yield global scale estimates of radiative fluxes that can be used for testing of numerical model flux estimates under a wide range of conditions. In this study, we focus on the Atlantic because it is relatively well sampled by supporting information (buoys, ships) and it is a region where coupled models have difficulty in getting the slope of the thermocline to have the correct sign and the sea surface temperature (SST) variability is difficult to reproduce.

3.2. Ground and Buoy Observations Used for Evaluation

[22] Several data sources on SW↓ and LW↓ observations over the oceans have been used. These include: Prediction and Research Moored Array in the Atlantic (PIRATA) [*Servain et al*., 1998; *Bourlès et al*., 2008; *McPhaden et al*., 1998]. To obtain a more robust statistics on errors, data from the Baseline Surface Radiation Network (BSRN) observing stations (available primarily over land) [*Ohmura et al*., 1998] (http://www.bsrn.awi.de/) have been also used.

3.3. Satellite Radiative Fluxes Used

[23] Details on the OAFlux radiative fluxes used in the intercomparison (both SW and LW) can be found in *Yu et al*. [2008]. Briefly, the WHOI OAFlux group uses radiative fluxes from the International Satellite Cloud Climatology Project (ISCCP)-FD product [*Rossow and Schiffer*, 1999; *Zhang et al*., 2004]. The ISCCP-FD model utilizes satellite observations from ISCCP (D1) cloud products gridded at a 280 km equal area grid and then transformed to a 2.5° equal angle grid. Details on the UMD SW and LW fluxes will be provided here.

3.3.1. UMD Shortwave Fluxes

[24] Two-independent estimates of SW↓ fluxes are available at UMD. One (UMD_DX_SW) is based on ISCCP DX observations [*Rossow and Schiffer*, 1999] as described in *Ma and Pinker* [2012] while the other (UMD_MODIS_SW) utilizes observations from MODIS Aqua and Terra as described by *Wang and Pinker* [2009]. There are known advantages to each data set. The SW↓ estimates based on ISCCP DX are available for a longer time period (1983–2009) at 3 hourly intervals while the MODIS based estimates started only around 2002, continue till present and have only two observations during daytime (from Terra and Aqua) and require assumptions on modeling the diurnal cycle. For longer term studies, there is a need to merge these two data sets. As will be shown in section 4.1, over oceans, the MODIS based daily products for both SW↓ and LW↓ are in better agreement with buoy observations than the UMD_DX based ones (additional evaluation of the SW↓ fluxes can be found in *Niu et al*. [2010] and *Pinker et al*. [2009]). Therefore, in this study, the MODIS estimates will be used in combination with the IFREMER turbulent fluxes to derive a satellite based estimate of the total net flux (Q_{net}).

3.3.2. UMD Longwave Fluxes

[25] A new approach for calculating downwelling surface longwave (LW↓) radiation under clear and all sky conditions [*Nussbaumer and Pinker*, 2012] is used here. It can be driven with auxiliary information from independent sources. The version used here is denoted as UMD_MODIS_LW↓ and is driven with a synthesis of the latest 1° resolution MODIS level-3 cloud parameters and information from the European Centre for Medium-Range Weather Forecasts (ECMWF) ERA-Interim model-analysis. The clear sky contribution in the model is based on the Rapid Radiative Transfer Model (RRTM) [*Mlawer et al*., 1997] while a statistical cloud structure model and parameterization determine the cloud contribution to LW↓. ECMWF ERA Interim Reanalysis model [*Berrisford et al*., 2009] parameters of vertical structure of temperature and humidity were used. It was shown that over oceans, the MODIS based product was in better agreement with buoy observations than if driven with the ISCCP DX cloud information (Figure 7). As discussed by *Nussbaumer and Pinker* [2012], the improved performance of this approach as compared to several widely used methodologies is due to a better estimate of cloud base height. Therefore, in this study, the MODIS estimates of LW↓ will be used. The most recent release of the Reynolds analysis [*Reynolds et al*., 2007] of sea surface temperature (SST) is used to compute LW↑ using equation (7) with emissivity of 0.98. In addition to the satellite SST retrievals from AVHRR and AMSR-E the Reynolds products assimilate observations from ships and buoys from the International Comprehensive Ocean-Atmosphere Data Set (ICOADS).

3.3.3. MODIS Data Used as Model Inputs

[26] Several products from the Moderate Resolution Imaging Spectroradiometer (MODIS) [*King et al*., 2003; *Platnick et al*., 2003] are being used for both SW and LW computations in the University of Maryland (UMD) models. These include Atmospheric Daily Global Product level-3 and MODIS Terra and Aqua Collection 5 monthly level-3 aerosol data and precipitable water. Missing MODIS data on precipitable water are replaced with information from the National Centers for Environmental Prediction (NCEP) Reanalysis Data [*Kistler et al*., 2001] while missing aerosol optical depths under cloudy conditions and over arid areas are filled with information from the Multi-angle Imaging Spectroradiometer (MISR) Component Global Aerosol Product (CGAS) [*Kahn et al*., 2001; *Martonchick et al*., 1998]. In the UMD_DX_SW scheme, the clear sky signal received by the satellite is used to derive the surface albedo as described by *Ma and Pinker* [2012]. In the UMD_MODIS_SW scheme, the albedo over oceans

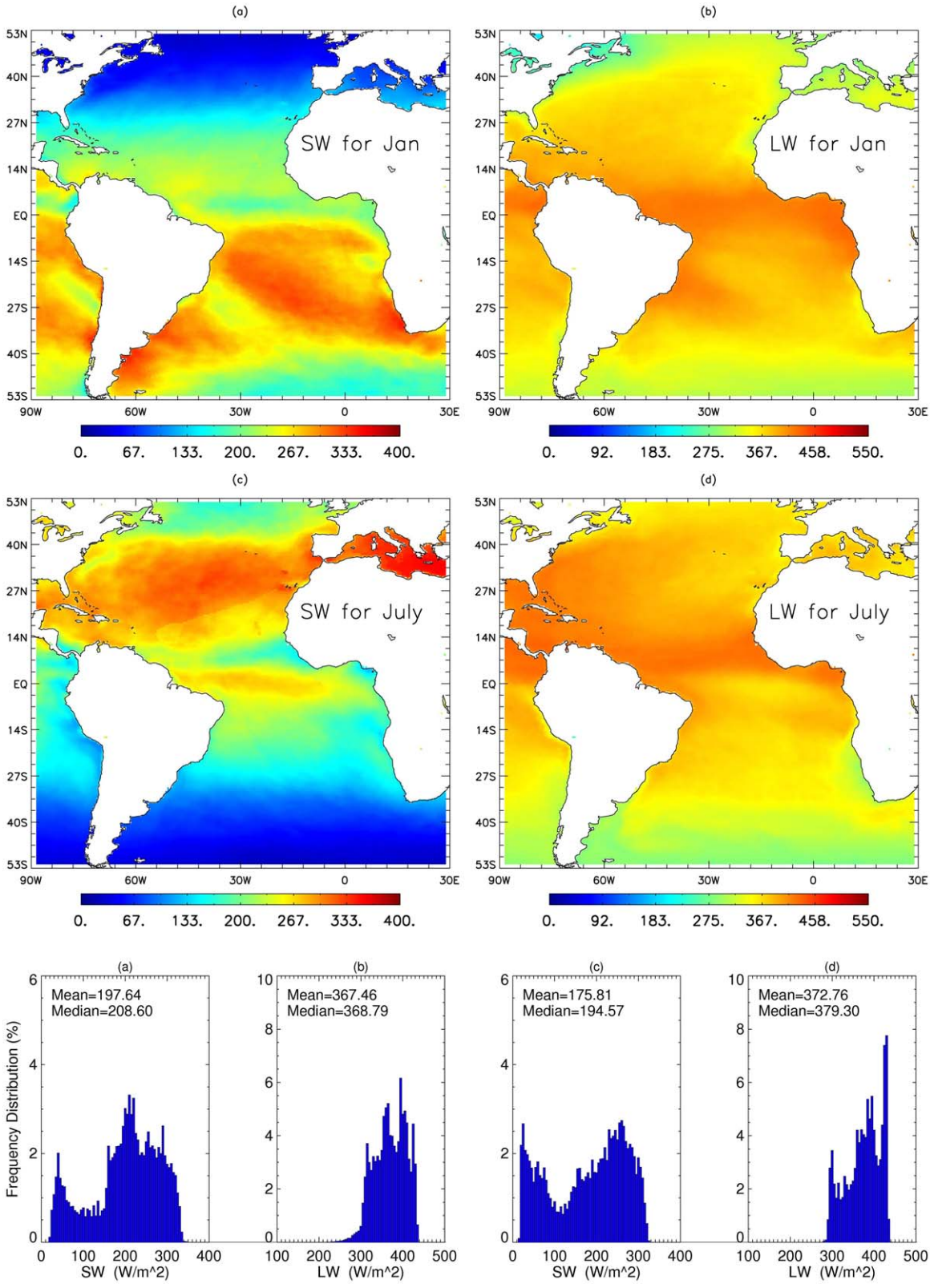

Figure 5. (top) Mean surface radiative fluxes as derived from UMD_MODIS_SW and UMD_MODIS_LW in W/m^2 (a) downward SW↓ for January, (b) downward LW↓ January, (c) downward SW↓ July, (d) downward LW↓ July for 2003–2005. (bottom) Histograms for above. In Figure 5b, you find marked the location for the three time series discussed in section 4.3.

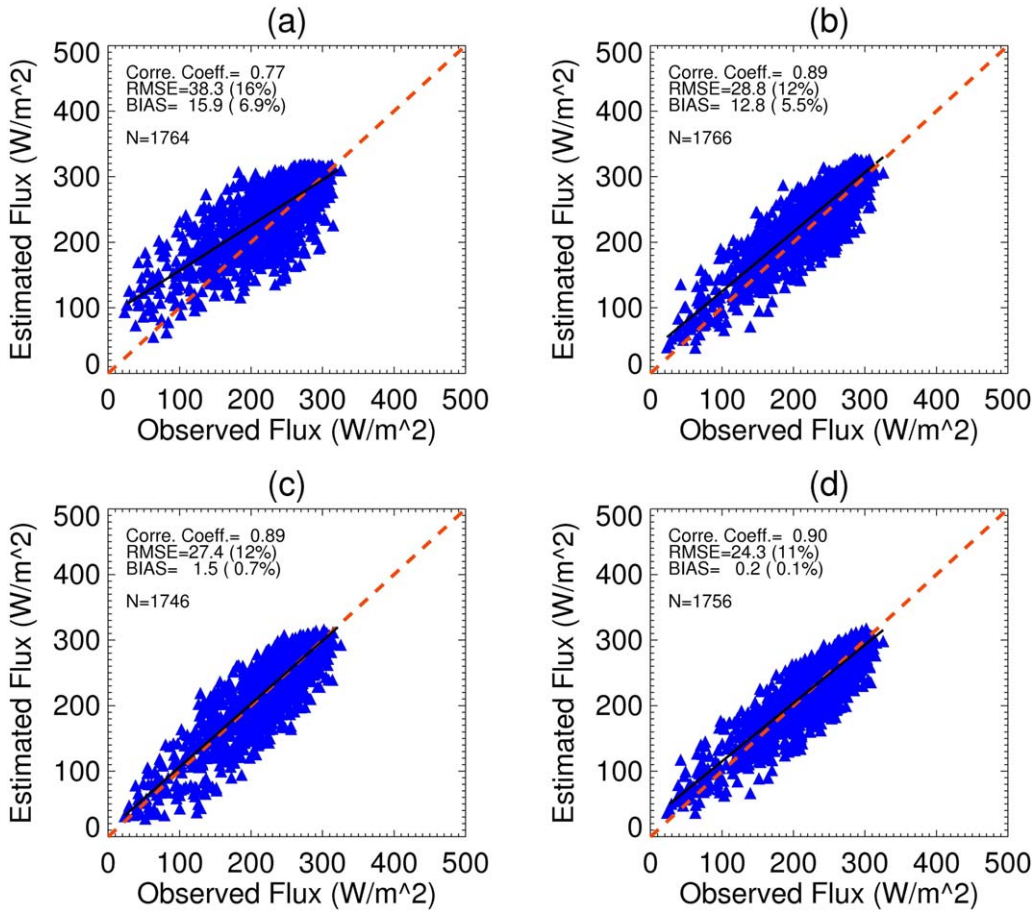

Figure 6. Evaluation of daily surface SW↓ radiative fluxes from satellite estimates against PIRATA buoys for 2004: (a) WHOI SW, (b) UMD_DX_SW, (c) UMD_MODIS_SW, and (d) UMD_MODIS_SW from 1 January 2003 to 31 December 2005 (cases eliminated: 1.1%).

that is used to compute K^* follows the approach of *Briegleb et al*. [1986].

4. Results

4.1. Radiative Fluxes

[27] In Figure 5, we present the mean radiative SW↓ and LW↓ fluxes at the sea surface, for 2003–2005 from UMD_-MODIS_SW and from UMD_MODIS_LW for: (a) SW↓ for January, (b) LW↓ for January, (c) SW↓ for July, and (d) LW↓ July. They clearly show the main known features of radiative fluxes; the SW↓ has mainly horizontal patterns and the associated maxima are located along the subtropical latitudes. For instance, at the northern areas SW↓ increases at about 100 W/m^2 between winter and summer seasons. However, as illustrated by histograms (Figure 5), on average, SW↓ loses about 20 W/m^2 between January and July mostly due to the loss of SW↓ at latitudes higher than 30°S. Except the low values in high latitudes, the minimum SW↓ values are found along the intertropical convergence zone (ITCZ). LW↓ seasonal variation is lower than what is found for SW↓. The highest values are mainly found along the ITCZ, and over north western areas during summer. Evaluation of daily surface downward SW↓ radiative fluxes from satellite estimates against PIRATA buoys for 2004 have been performed and are illustrated in Figure 6. In addition to the evaluation of the SW↓ data used by WHOI, results for both UMD products are shown, namely, ISCCP and MODIS based (to provide rationale for the selection of the MODIS products for the intercomparison with the WHOI OAFlux products). As evident from the figure, the range of the RMSE and Bias errors for the 2004 daily values of the ISCCP based products range between 30–40 W/m^2 and 13–16 W/m^2, respectively. The MODIS products were evaluated also for an expanded period during 2003–2005, showing a RMSE and Bias in the ranges of 25–27 and 1.3–3.0 W/m^2, respectively. It is believed that the major reason for the differences between the products is due to differences in cloud detection capabilities of the two observing systems, MODIS having 36 channels while the ISCCP products are based on 3–5 channels only [*Rossow et al*., 1993; *Stubenrauch et al*., 2013].

[28] Buoy observations of LW↓ fluxes are very limited. Therefore, initial evaluation of daily mean surface LW↓ flux estimated with the UMD_MODIS_LW and UMD_DX_LW at 1° spatial resolution was conducted against 18 BSRN stations for 2007 as reported on by *Nussbaumer and Pinker* [2012]. Evaluation of daily mean surface LW flux estimated with UMD_MODIS_LW and UMD_DX_LW models at 1° spatial resolution against all PIRATA buoy observations for

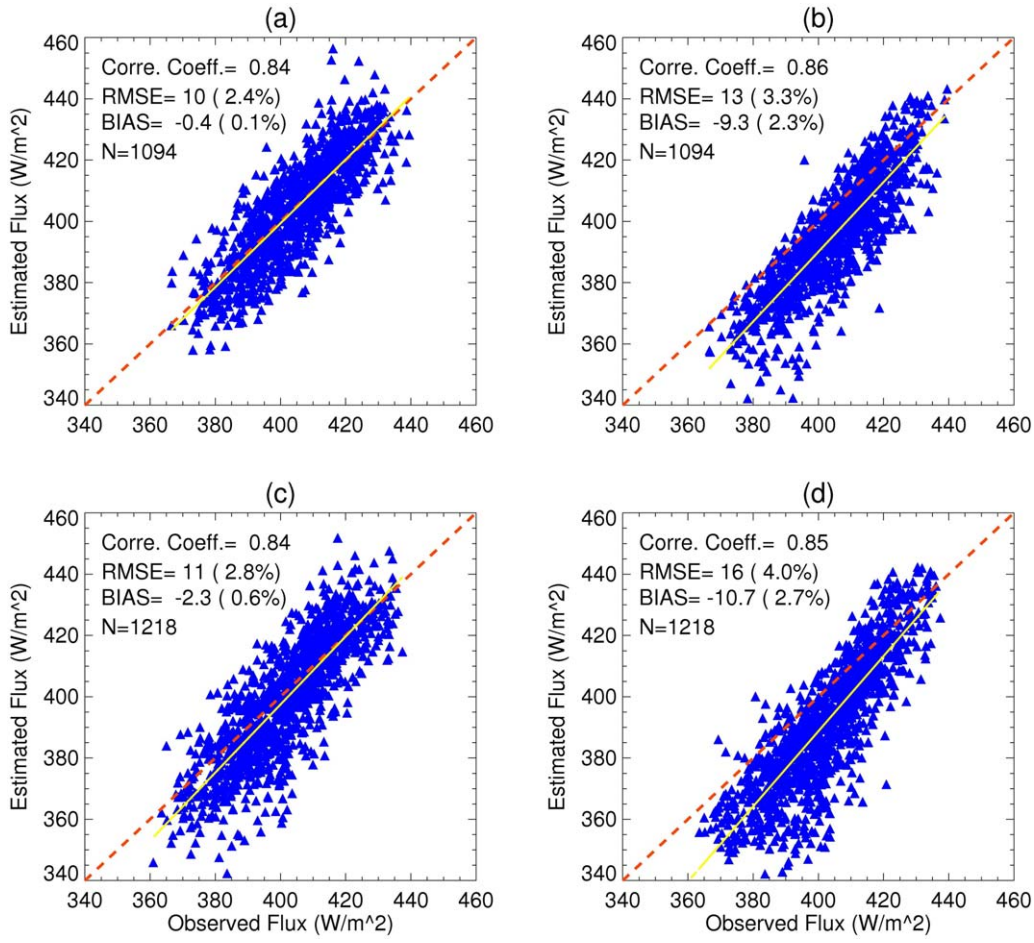

Figure 7. Evaluation of daily mean surface LW↓ flux as estimated from UMD_MODIS_LW and UMD_DX_LW models at 1° spatial resolution against PIRATA buoy that measure LW↓ radiation for the years 2007 and 2008. Location of buoys: 0°N, 23°W; 10° S, 10°W; 12°N, 23°W; and 15°N, 38°W. (a) UMD_MODIS_LW for 2007. (b) UMD_DX_LW for 2007. (c) UMD_MODIS_LW for 2008. (d) UMD_DX_LW for 2008.

the years 2007 and 2008 is presented in Figure 7. Location of buoys: 0°N, 23°W; 10°S, 10°W; 12°N, 23°W; 15°N, 38°W. (a) UMD_MODIS_LW 2007; (b) UMD_DX_LW 2007; (c) as (a) for 2008; (d) as (b) for 2008. As will be shown in the evaluation results, the MODIS estimates of radiative fluxes are in better agreement with the ground observations than those from the UMD_DX_LW products (for both SW and LW). Therefore, in formulating the statistical values of differences between the two approaches, only the MODIS estimates are used.

4.2. Comparison of Fluxes From UMD and OAFlux

4.2.1. Comparison of Net (Q^*) Radiative Fluxes

[29] In Figure 8, illustrated are net radiative flux differences (Δ) between UMD_MODIS and data used by WHOI (OAFlux_ISCCP-FD) during January and July of 2003–2005 (a) net SW (K^*) UMD_MODIS_SW—net SW (K^*) from OAFlux_ISCCP-FD for January; (b) net LW (L^*) UMD_MODIS_LW—net LW (L^*) from OAFlux_ISCCP-FD for (c) as (a) for July; (d) as (b) for July. Histograms of differences are also presented. The negative differences in SW↓ fluxes can be attributed to differences in cloud amounts used in the two products, namely, there are less clouds in the ISCCP observations than detected by MODIS, which will results in higher estimates of SW↓ in the OAFlux_ISCCP-FD products [*Pincus et al*., 2012; *Stubenrauch et al*., 2013]. According to *Pincus et al*. [2012] who compared clouds from MODIS and ISCCP, relative to ISCCP, clouds observed by MODIS tend to be slightly more frequent, lower in the atmosphere (and warmer), and optically thicker. They also point out that the largest differences between these two products can be traced to different approaches to partly cloudy pixels, which MODIS excludes and ISCCP treats as homogeneous. The partly cloudy pixels cover roughly 15% of the planet and account for most of the optically thinnest clouds. Less clouds in the ISCCP based products would result in lower LW↓ fluxes (more LW↓ can escape to space) which will make the difference between the two products positive, as seen in Figures 8b and 8d.

4.2.2. Net Surface Heat Flux (Radiative + Latent + Sensible) (Q_{net})

[30] Net heat (Q_{net}) fluxes as calculated in numerical weather prediction models (particularly NCEP and ECMWF) are used for ocean circulation, water mass

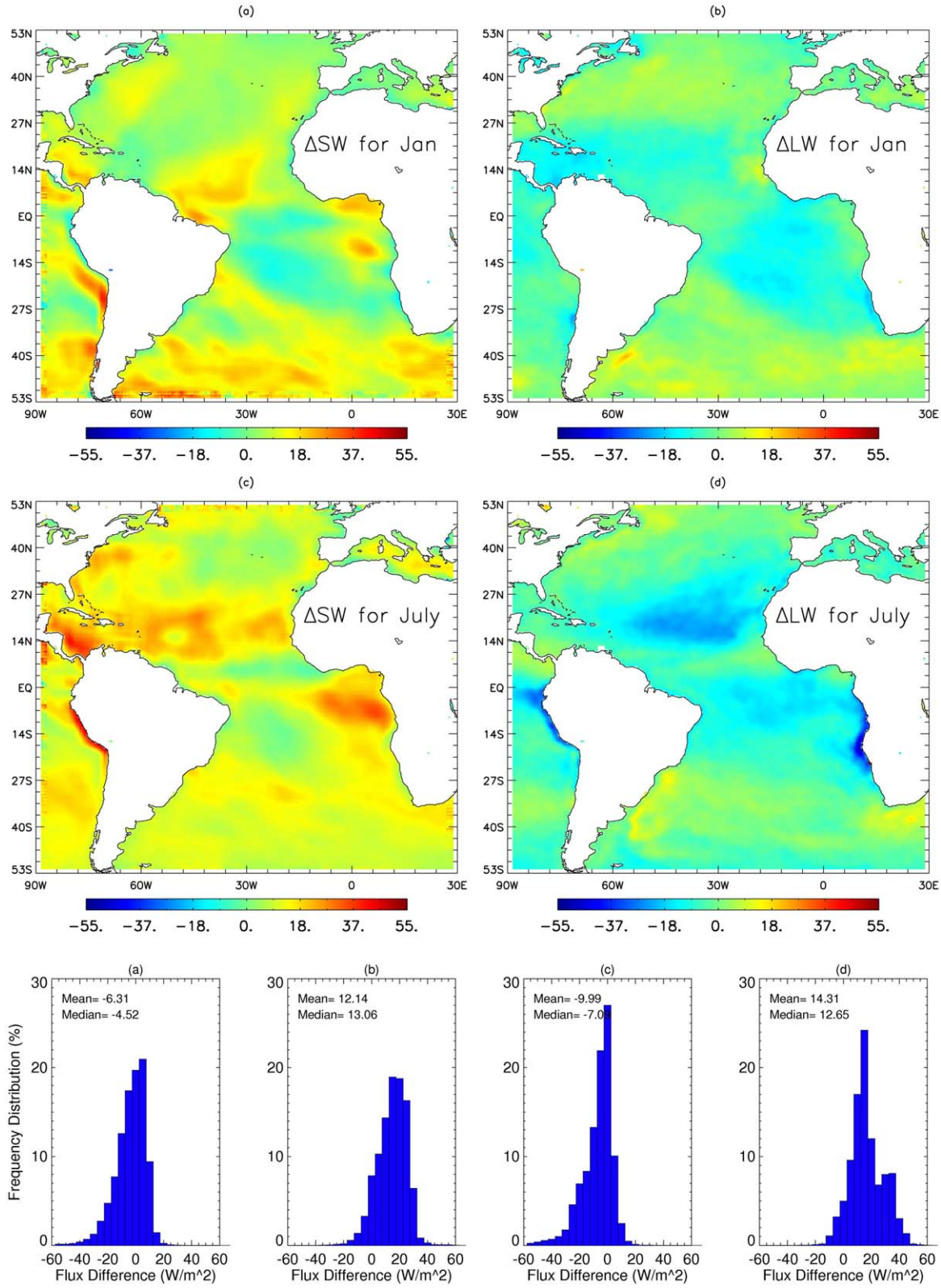

Figure 8. (top) Net radiative flux (Q^*) differences (Δ) between UMD_MODIS and data used by WHOI (WHOI OAFlux) during January and July of 2003–2005 (a) net SW (K^*) UMD_MODIS—net SW (K^*) from WHOI for January, (b) net LW (L^*) UMD_MODIS—net LW (L^*) from WHOI for January, (c) as Figure 8a for July, and (d) as Figure 8b for July. (bottom) Histogram of differences for above.

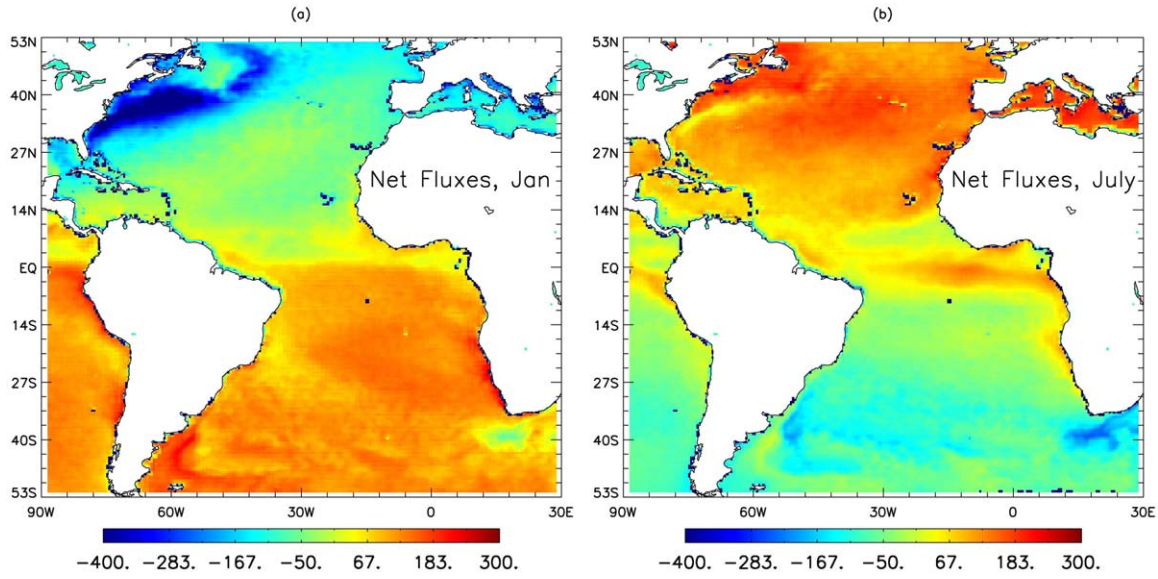

Figure 9. Net fluxes (radiative and turbulent, Q_{net}) from UMD_MODIS_SW, UMD_MODIS_LW and IFREMER turbulent [*Bentamy et al*., 2012] for (a) January; (b) for July during 2003–2005.

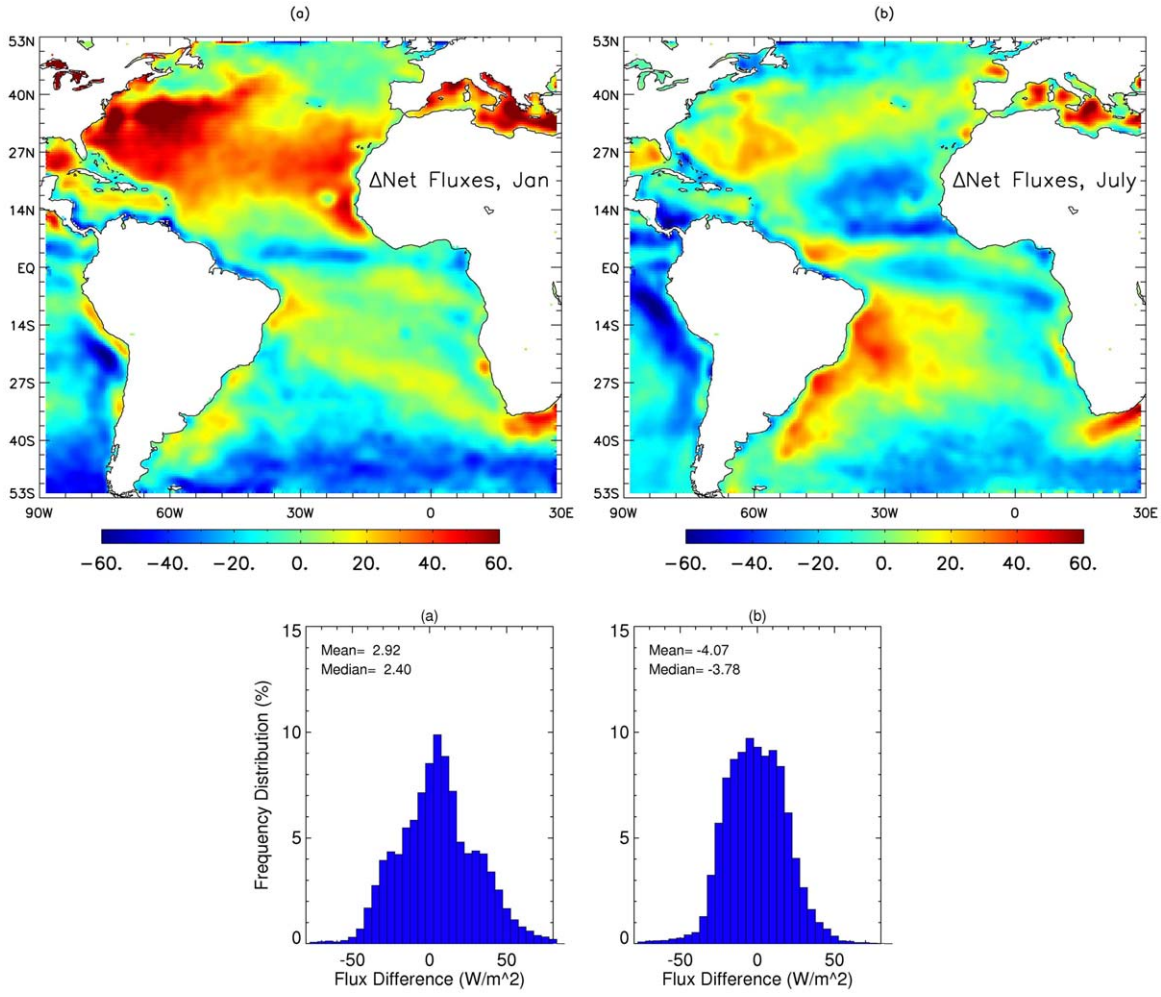

Figure 10. (top) Difference in total net flux (radiative and turbulent, Q_{net}) over the Atlantic from UMD_MODIS (SW and LW) and IFREMER turbulent minus OAFLUX total net flux (Q_{net}) during 2003–2005: (a) January and (b) July. (bottom) Histogram of differences for above.

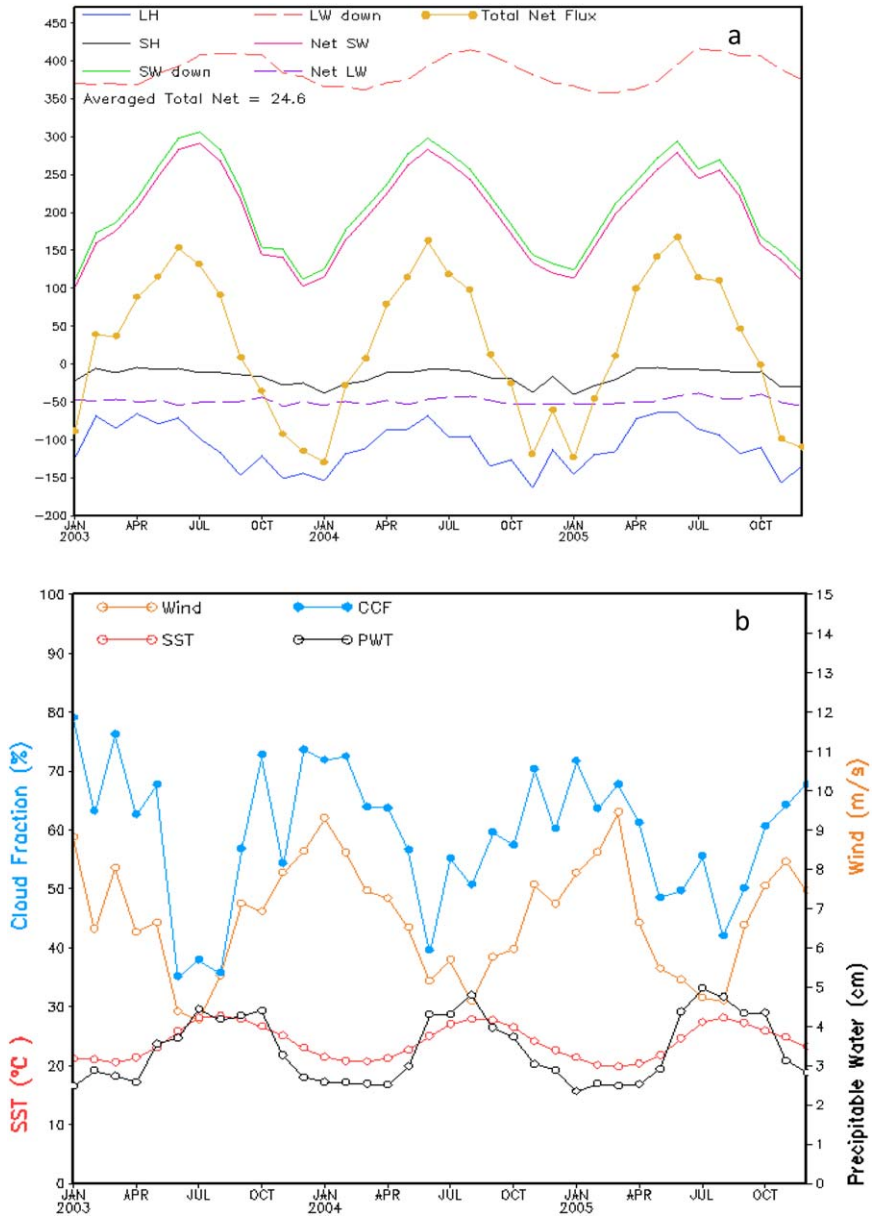

Figure 11. (a) Time series of turbulent flux components (LH and SH), SW↓ and LW↓ and net radiative fluxes (K^* and L^*) and total net fluxes (turbulent and radiative, Q_{net}) averaged for 2003–2005 at a: 30°N and 60°W and (b) wind speed, SST, cloud fraction (CCF), and precipitable water (PWT) for the same location and time period.

formation climate variability studies, and other related projects. Satellite estimates of the net fluxes can contribute to the evaluation of numerical models, while temperature, humidity, wind, and radiation measurements from the PIRATA, ODAS, and WHOI-IMET buoy networks in the Tropical Atlantic can be used to evaluate the satellite estimates. The radiative fluxes are an important component of the total heat budget and as such, need to be well known. Adding the net radiative fluxes to the turbulent heat fluxes (latent and sensible) results in Q_{net}:

$$Q_{net} = Q* + LH + SH \quad (8)$$

where

$$Q* = (K* + L*) \quad (9)$$

[31] A positive Qnet indicates heating of the ocean. We illustrate this sum in Figures 9 for the average January and July of 2003–2005. As expected the seasonal patterns are clearly depicted. The ocean gains heat in southern areas during January and in northern regions in July. This seasonal variation is illustrated in net heat variation along the Gulf Stream. The ocean loses and gains heat in winter and summer seasons, respectively. The differences between the sum of the IFREMER turbulent flux + UMD radiative net flux (Q^*) and the net total flux from the OAFlux product is presented in Figure 10. Clearly, there are major differences in the Gulf Stream region and in the coastal upwelling

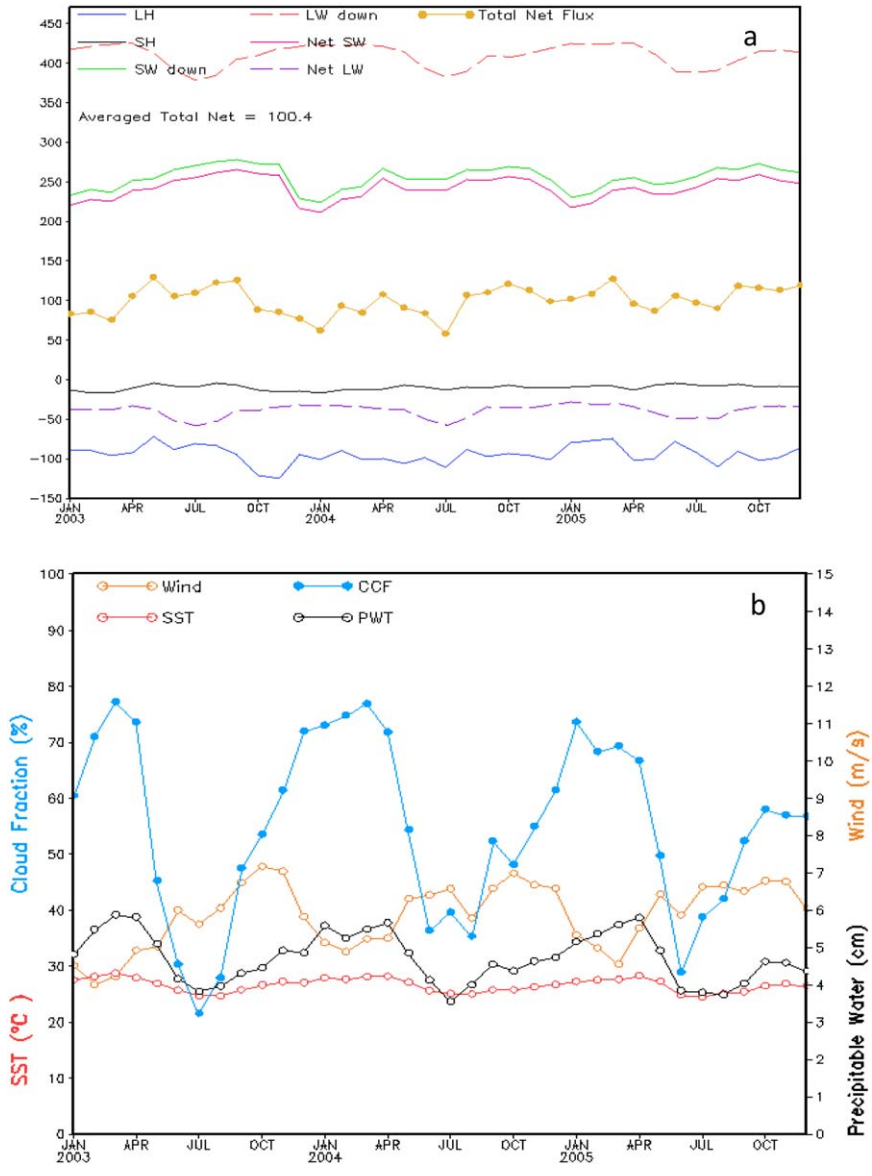

Figure 12. (a) Time series of turbulent flux components (LH and SH), SW↓ and LW↓ and net radiative fluxes (K^* and L^*), and total net fluxes (turbulent and radiative, Q_{net}) averaged for 2003–2005 at specific locations: 0° and 20°W and (b) wind speed, SST, cloud fraction (CCF), and precipitable water (PW) for the same location and time period.

regions west of continents where our product implies heating. East of South America, there are large differences between these products and they are of opposite sign. Many of the large differences in the regions of subtropical highs, the Gulf Stream, in foggy upwelling regions may be due to problems with defining clouds in both products. To look into the influence of the cloudiness, the atmospheric humidity, wind speed, and SST, we analyze time series of these variables and the flux terms for a three select points (these locations are shown by red *'s in Figure 5b).

4.3. Time Series at Selected Locations

[32] It is of interest to understand the time evolution and relationship between the various flux components across the Atlantic Basin. We illustrate findings at three locations representing the upper north and south domains of the basin as well as an equatorial location (Figures 11a, 12a, and 13a). For example, series of turbulent flux components (LH and SH), SW↓ and LW↓ and net radiative fluxes and total net flux Q_{net} (turbulent and radiative) averaged for 2003–2005 at 30°N and 60°W are illustrated in Figure 11a; similar quantities for 0°N, 20°W and 40°S, 50°W are presented in Figures 12 and 13. Total precipitable water (PWT), Cloud Cover Fraction (CCF), wind speed, and SST appear separately for clarity as Figures 11b, 12b, and 13b. From the time series constructed from monthly averages of the variables at select points, one finds many instructive insights concerning the relationships between the atmospheric and sea surface variables, such as total precipitable water (PWT), Cloud Cover Fraction (CCF), wind speed,

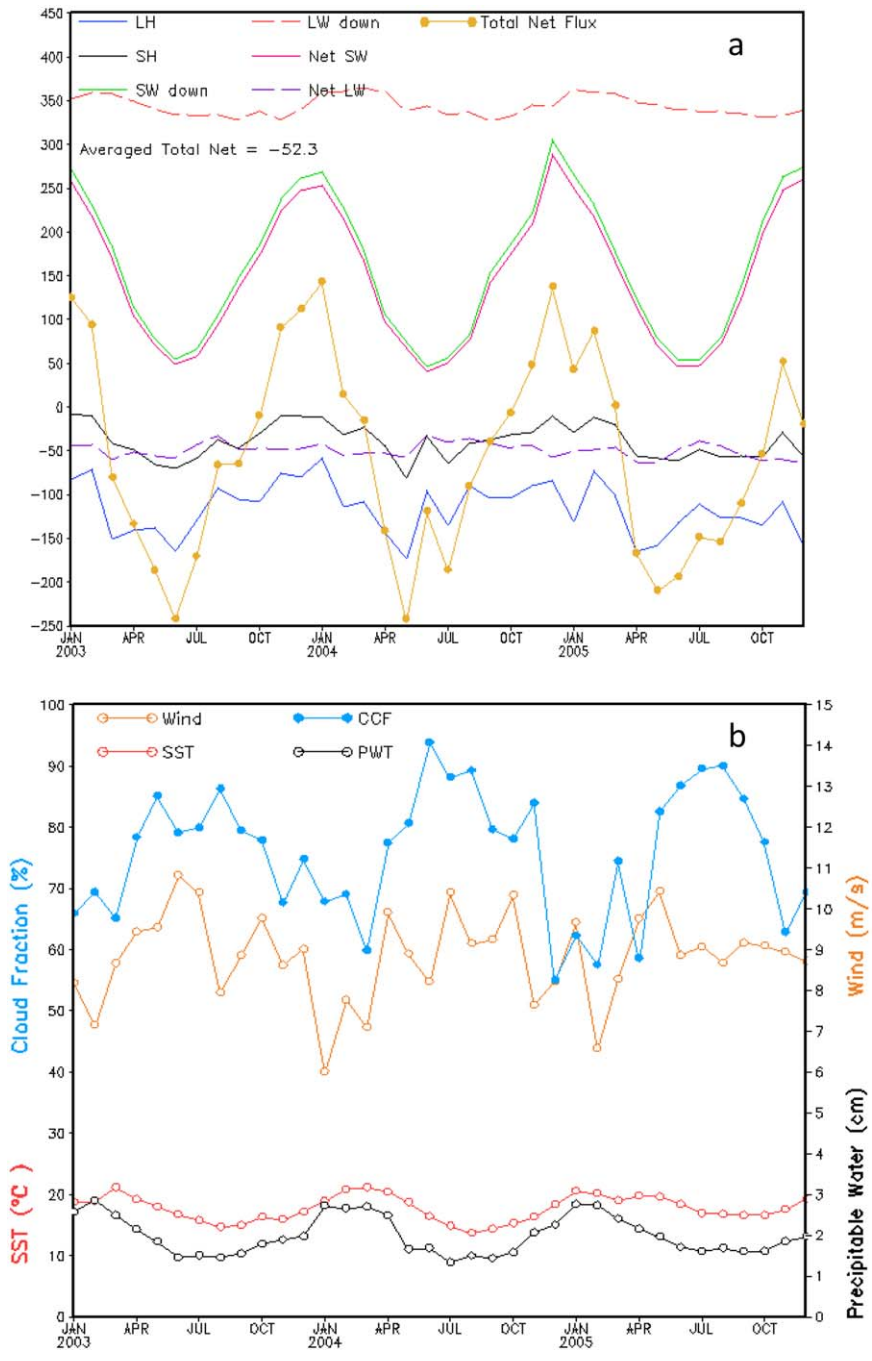

Figure 13. (a) Time series of turbulent flux components (LH and SH), SW↓ and LW↓ and net radiative fluxes (K^* and L^*), and total net fluxes (turbulent and radiative, Q_{net}) averaged for 2003–2005 at: 40°S and 50°W and (b) wind speed, SST, cloud fraction (CCF), and precipitable water (PW) for the same location and time period.

Table 1. Variables Used to Derive IFREMER and WHOI Turbulent Heat Fluxes (Latent and Sensible) and Their Origin

Variable	Source for IFREMER	Source for WHOI
Air temperature	Estimated from Era Interim reanalyses	NCEP, ECMWF reanalyses
Sea surface temperature	*Reynolds et al*. [2007]	NCEP, ECMWF reanalyses, *Reynolds et al*. [2007]
Surface wind speed	EQuickSCAT scatterometer	NCEP, ECMWF reanalyses, SSM/I and AMSR-E radiometers, QuickSCAT scatterometer
Specific air humidity	Estimated from SSM/I brightness temperature using the *Bentamy et al*. [2013] model	NCEP, ECMWF reanalyses, product from *Chou et al*. [1997] using SSM/I column water vapor retrievals

Table 2. Mean and Median Values of Latent (LH) and Sensible Heat (SH) Fluxes for January and July as Available From IFREMER [*Bentamy et al*., 2012] for 2003–2005[a]

Parameter	Mean-Jan.	Mean-Jul.	Median-Jan.	Median-Jul.
LH	102.39	91.33	98.58	96.59
SH	19.03	13.25	11.84	11.76
SW↓: MODIS	197.64	175.81	208.60	194.57
LW↓: MODIS	367.46	372.76	368.79	379.30
Net SW↓Flux: K*	184.65	164.00	194.61	181.19
Net LW↓Flux: L* (both from MODIS)	−42.54	−38.49	−43.97	−38.93

[a]Mean and median values of downwelling surface radiative fluxes for January and July from UMD_MODIS for SW↓ and UMD_MODIS for LW↓ for 2003–2005; mean and median values of net surface radiative fluxes (Q*) for January and July from UMD_MODIS for SW↓ and UMD_MODIS for LW↓ for 2003–2005 (values are given in W/m^2).

SST, and the SW↓, LW↓, and net radiative (Q*) and net turbulent (T*) fluxes at the sea surface, to be detailed in what follows.

4.3.1. Analysis at 30°N and 60°W

[33] At 30°N, 60°W the net heat flux is dominated by the net short wave flux (K*) with an in-phase variation of the evaporation/latent heat flux (Figure 11a). SH and L* are very flat and almost constant throughout the 3 years. An interesting feature of the plots of CCF and PWT (Figure 11b) is that they show variations completely out-of-phase with each other. CCF is also out-of phase with the SW down (Figure 11a) as expected. Surface wind speed variations are not exactly in phase with the LH, but seem to lead by a couple of months in each year. SST and PWT vary in phase, which makes physical sense, but are almost out-of phase with the wind speed variations. This example clearly shows how complex the evaluation of net heat flux is.

4.3.2. Analysis at 0°, 20°W

[34] At the equator the radiative flux terms remain rather flat throughout the 3 years (Figure 12a). At other locations along the equator they may show a stronger signal in the radiative fluxes of the moving Inter-Tropical Convergence Zone (ITCZ). Here, Figure 12b shows the effect of the ITCZ in the CCF, which varies from 70 to 80% at the peaks in all 3 years during February–March, to a low of 20–30% for the monthly averages of July. PWT ranges between 4 and 5 cm, which explains why the K*, L*, and LH and SH fluxes are so flat and of low magnitude.

4.3.3. Analysis at 40°S and 50°W

[35] At this southery location, all the flux terms presented show annual variations in phase with the net flux varying between about +140 W/m^2 and about −240 W/m^2. Wind speed is quite high in the mean in this southern Atlantic location ranging between 7 and 9 m s^{-1}. Cloud fraction stays at about 70–90%, while SST shows a 20°C ± 2°C and shows variations in phase with PWT having low values of order 1.5–2.8 cm.

5. Conclusions

[36] The oceanic heat storage depends on the surface net heat flux and the horizontal advection and vertical mixing; the amount of heat stored in the sea (upper layers) will increase or decrease accordingly. We have shown that over the Atlantic Ocean the net heat input to the upper ocean from surface fluxes, exhibits both temporal and spatial variations that can be large and that the two prototypes of flux estimates used in this study differ substantially in several regions. In oceanographic studies, radiative fluxes have often been either ignored or taken from simple climatology or parameterizations. We have shown here that uncertainties in *the net radiative heat flux* at the sea surface can be as large as variations in the *turbulent heat flux*. Reasons for these differences and their temporal and spatial variations are numerous and the key ones have been identified. There are difficulties in comparing flux estimates both turbulent and radiative due to inconsistencies in methodology and data input. An obvious one is the difference in reference height in numerical models, buoy, and satellite estimates of surface variables. This problem was addressed in an earlier paper [*Santorelli et al*., 2011], but some standardization in future satellite retrievals, model formulations, and buoy calculations would be helpful for creating more consistent climate records. In our approach, we used two very different prototypes of approaches (satellite versus more model and assimilation based methods) and illustrated that for turbulent fluxes the two methods are converging to similar results while the differences in radiative fluxes are larger. It is believed that future work on radiative fluxes could benefit from higher resolution observations in time and space, improved resolution of the diurnal cycle, improved information on aerosols for the SW↓ fluxes and better characterization of cloud base height, for the LW↓ fluxes. A summary of what was learned is given in Tables 2 and 3.What is also evident from the time series analyzed and presented in Figures 11–13, is that the Atlantic Ocean has very different characteristic regions that should be analyzed independently. The uniqueness of this study is that we have

Table 3. Differences in Mean and Median Values of Latent (LH) and Sensible (SH) Heat Fluxes for January and July as Available From IFREMER [*Bentamy et al*., 2013] and WHOI OAFlux [*Yu et al*., 2008] for 2003–2005[a]

Parameter	Mean-Jan.	Mean-Jul.	Median-Jan.	Median-Jul.
ΔLH (IF − WH)	−2.27	2.85	0.98	3.05
ΔSH (IF − WH)	5.4	5.64	4.9	5.23
ΔSW↓ (DX − MO)	8.15	12.64	7.53	11.82
ΔLW↓ (DX − MO)	−1.55	−5.41	−0.26	−4.61
ΔNet SW↓ (K*) ($UMD_{\_MO}$ − WH)	−6.31	−9.99	−4.52	−7.02
ΔNet LW↓(L*) (UMD_{MO} − WH)	12.14	14.31	13.06	12.65
ΔNet (rad + turb)(Q_{net}) UMD_{MO} − WH)	2.92	−4.07	2.40	−3.78

[a]Differences in mean and median values of SW↓ and LW↓ fluxes as derived from UMD_DX_SW v3.3.3 minus UMD_MODIS_SW and UMD_DX_LW minus UMD_MODIS_LW for 2003–2005 for January and July; differences in mean and median net SW↓ (K*) radiative fluxes (Δ) between UMD_MODIS and data used by WHOI (WHOI OAFlux) during January and July of 2003–2005 (net SW↓ (K*) UMD_MODIS– net SW↓ (K*) from WHOI and net LW↓ (L*) UMD_MODIS– net LW↓ (L*) from WHOI); difference in mean and median total net flux (radiative and turbulent) over the Atlantic from UMD_MODIS (SW↓ and SW↓) and IFREMER turbulent—WHOI total net flux during 2003–2005 for January and July.

looked in detail at both radiative and turbulent heat fluxes over the Atlantic Ocean, with emphasis on the satellite data used as a basis for the estimates.

[37] In an earlier paper, *Josey et al*. [1999] discuss the difficulties in obtaining and evaluating turbulent fluxes at the sea-air interface. They argue that a flux of 10 W/m^2 over 1 year if stored in the top 500 m of the ocean, would heat that entire layer by about 0.15°C. Temperature changes on a decadal time scale are at most a few tenths of a degree, so the global mean budget must balance to better than a few W/m^2. They conclude that at that time such accuracy could not be achieved. During a recent CLIVAR GSOP Workshop on Observing System Evaluation and Intercomparison [*Oke et al*., 2011] a plan was developed on intercomparison of various parameters such as the total net flux to be based on about 19 numerical models. Results were reported at the CLIVAR GSOP/GODAE Ocean Reanalyses Intercomparison Workshop [*Balmaseda et al*., 2013]. Positive imbalances in global surface heating ~5 W/m^2 (1993–2009) were found. This is far larger than the observed global heat content change above 3000 m (<1 W/m^2), but down from the 25 to 20 W/m^2 from previous studies. While these estimates are quite informative, global averaging does conceal difficulties in certain regions due to averaging. Table 2 presents averages between 45°S and 45°N, of the various fluxes. As shown, the net SW Flux is the dominant term in both seasons and represents a gain of energy while the net LW is much smaller and represents a loss in both seasons. Approximately, the net radiative fluxes balance the net turbulent fluxes. From Table 3, it can be learned the net LW differences between the two approaches dominate the total differences (12 and 14 W/m^2 in summer and winter). The total net differences between the two approaches is quite small (2.92–4.07 W/m^2 in summer and winter, respectively) which is about half of the values presented from the model comparisons as described in *Balmaseda et al*. [2013]. It is therefore recommended that analyses from "observations" as well as from models need to be conducted at regional scales in areas of climatic significance.

[38] **Acknowledgments.** We thank NSF for support under grants ATM0631685 to the University of Maryland and grant ATM0631792 to the University of Miami under which this work was initiated. The analysis was completed under NASA grant NNX13AC12G, the Energy and Water Cycle Study (NEWS) program. The work also benefited from support under NASA grant NNX08AN40A from the Science Mission Directorate-Division of Earth Science. Thanks are due to the NASA GES DISC Giovanni for the MODIS data, to the various MODIS teams that produced data used in this study, to the Baseline Surface Radiation Network for observations used in the evaluation, to the NASA Langley Research Center Atmospheric Science Data Center for providing the ISCCP DX data and to Lisan Yu of Woods Hole, who provided the OAFlux data and the daily averaged radiative fluxes from ISCCP-FD. We acknowledge the TAO Project Office of NOAA/PMEL for providing data from the Pilot Research Moored Array in the Tropical Atlantic (PIRATA) that were used in this study. We thank Chuan Li for technical assistance. A. Bentamy wishes to thank S. Grodsky, University of Maryland (USA), A. Mestas_-Nuñez, University of Corpus Christi (USA), B. Blanke, University of Bretagne Ouest (UBO/France), and F. Desbiolles, IFREMER/LOS (France) and UBO, for their comments, suggestions and encouragement that led to improvement in turbulent flux estimates derived from remotely sensed data. He also thanks F. Paul, D. Croizé-Fillon, J. F. Piollé, and IFREMER/CERSAT for data processing support and is grateful to ECMWF, EUMETSAT, CERSAT, JPL, ISRO, NOAA, NOCS, Météo-France, NDBC, PMEL, and UK MetOffice for providing numerical, satellite, and in situ data. We are grateful to two anonymous reviewers for very helpful and constructive comments.

References

Angell, J. K. (1988), Impact of E1 Nino on the delineation of tropospheric cooling due to volcanic eruptions, *J. Geophys. Res.*, *93*, 3697–3704.

Angell, J. K., and J. Korshover (1985), Surface temperature changes following the six major volcanic episodes between 1780 and 1980, *J. Clim. Appl. Meteorol.*, *24*, 937–951.

Balmaseda, M. A., F. Hernandez, T. Lee, A. Storto, M. Valdivieso, and K. Wilmer-Becker (2013), Introduction to the Ocean Reanalysis Intercomparison project, CLIVAR GSOP/GODAE Ocean Reanalyses Intercomparison Workshop ECMWF, Reading, U. K., 1–3 July.

Bentamy, A., K. B. Katsaros, A. M. Mestas-Nuñez, W. M. Drennan, E. B. Forde, and H. Roquet (2003), Satellite estimates of wind speed and latent heat flux over the global oceans, *J. Clim.*, *16*, 637–656.

Bentamy, A., L.-H. Ayina, W. Drennan, K. Katsaros, A. M. Mestas-Nuñez, and R. T. Pinker (2008), 15 years of ocean surface momentum and heat fluxes from remotely sensed observations, *FLUXNEWS 5*, pp. 14–16, World Clim. Res. Program., Geneva, Switzerland. [Available at http://sail.msk.ru/newsletter/fluxnews_5_final.pdf.].

Bentamy, A., S. A. Grodsky, K. Katsaros, A. M. Mestas-Nuñez, B. Blanke, and F. Desbiolles (2013), Improvement in air-sea flux estimates derived from satellite observations, *Int. J. Remote Sens.*, *34*(14), 5243–5261, doi:10.1080/01431161.2013.787502.

Berrisford, P., D. Dee, K. Fielding, M. Fuentes, P. Kållberg, S. Kobayashi, and S. Uppala (2009), The ERA-Interim archive, Version 1.0, *ERA Rep. Ser*., Eur. Cent. for Medium Range Weather Forecasts, Reading, U. K.

Bock, O., F. Guichard, S. Janicot, J. P. Lafore, M.-N. Bouin, and B. Sultan (2007), Multiscale analysis of precipitable water vapor over Africa from GPS data and ECMWF analyses, *Geophys. Res. Lett.*, *34*, L09705, doi:10.1029/2006GL028039.

Bourras, D. (2006), Comparison of five satellite-derived latent heat flux products to moored buoy data, *J. Clim.*, *19*, 6291–6313.

Bourassa, M. A., et al. (2013), high-latitude ocean and sea ice surface fluxes: Challenges for climate research, *Bull. Am. Meteorol. Soc.*, *94*, 403–423.

Bourlès, B., et al. (2008), The PIRATA Program: History, accomplishments, and future directions, *Bull. Am. Meteorol. Soc.*, *89*(8), 1111–1125, doi:10.1175/2008BAMS2462.1.

Briegleb, B. P., P. Minnis, V. Ramanathan, and E. Harrison (1986), Comparison of regional clear sky albedos inferred from satellite observations and model computations, *J. Clim. Appl. Meteorol.*, *25*(2), 214–226, doi:10.1175/1520-0450.

Chou, S.-H., C.-L. Shie, R. M. Atlas, and J. Ardizzone (1997), Air-sea fluxes retrieved from Special Sensor Microwave Imager data, *J. Geophys. Res.*, *102*, 12,705–12,726.

Driscoll, S., A. Bozzo, L. J. Gray, A. Robock, and G. Stenchikov (2012), Coupled Model Intercomparison Project 5 (CMIP5) simulations of climate following volcanic eruptions, *J. Geophys. Res.*, *117*, D17105, doi:10.1029/2012JD017607.

Emanuel, K. A. (1988), The maximum intensity of hurricanes, *J. Atmos. Sci.*, *45*(7), 1143–1155.

Fairall, C. W., E. F. Bradley, J. E. Hare, A. A. Grachev, and J. B. Edson (2003), Bulk parameterization of air-sea fluxes: Updates and verification for the COARE3.0 algorithm, *J. Clim.*, *16*, 571–591.

Foltz, G. R., S. A. Grodsky, J. A. Carton, and M. J. McPhaden (2003), Seasonal mixed layer heat budget of the tropical Atlantic Ocean, *J. Geophys. Res.*, *108*(C5), 3146, doi:10.1029/2002JC001584.

Gleckler, P. J., T. M. L. Wigley, B. D. Santer, J. M. Gregory, K. Achutarao, and K. E. Taylor (2006), Volcanoes and climate: Krakatoa's signature persists in the ocean, *Nature*, *439*, 675.

Graber, H. C., E. A. Terray, M. A. Donelan, W. M. Drennan, J. C. Van Leer, and D. B. Peters (2000), ASIS—A new air-sea interaction spar buoy: Design and performance at sea, *J. Atmos. Oceanic Technol.*, *17*, 708–720, doi:10.1175/1520-0426(2000)017<0708:AANASI>2.0.CO;2.

Grodsky, S. A., A. Bentamy, J. A. Carton, and R. T. Pinker (2009), Intraseasonal latent heat flux based on satellite observations, *J. Clim.*, *22*, 4539–4556.

Hastenrath, S. (1984), Interannual variability and annual cycle: Mechanisms of circulation and climate in the tropical Atlantic Sector, *Mon. Weather Rev.*, *112*, 1097–1107, doi:10.1175/1520-0493(1984)112<1097:IVAACM>2.0.CO,2.

Hauser, D., et al. (2003), The FETCH experiment: An overview, *J. Geophys. Res.*, *108*(C3), 8053, doi:10.1029/2001JC001202.

Hu, Q., S. Feng, and R. J. Oglesby (2011), Variations in North American summer precipitation driven by the Atlantic Multidecadal Oscillation, *J. Clim.*, *24*, 5555–5570, doi:10.1175/2011JCLI4060.1.

Hurrell, J. W., and C. Deser (2009), North Atlantic climate variability: The role of the North Atlantic Oscillation, *J. Mar. Syst.*, *79*(3–4), 231–244.

Intergovernmental Panel on Climate Change (2007), Climate Change 2007: The physical science basis, in *Contribution of Working Group I Contribution to the Fourth Assessment Report of the IPCC*, edited by S. Solomon et al., Cambridge Univ. Press, New York.

Jackson, D. L., G. A. Wick, and F. R. Robertson (2009), Improved multisensory approach to satellite-retrieved near-surface specific humidity observations, *J. Geophys. Res.*, *114*, D16303, doi:10.1029/2008JD011341.

Josey, S. A., E. C. Kent, and P. K. Taylor (1999), The Southampton Oceanography Centre (SOC) ocean-atmosphere heat, momentum and freshwater flux atlas, *SOC Rep. 6*, 30 pp., Figs. 5.1. [Available from the Library, Southampton Oceanogr. Cent., Eur. Way, Southampton, U. K.]

Kahn, R., P. Banerjee, and D. McDonald (2001), The sensitivity of multiangle imaging to natural mixtures of aerosols over ocean, *J. Geophys. Res.*, *106*, 18,219–18,238, doi:10.1029/2000JD900497.

King, M. D., W. P. Menzel, Y. J. Kaufman, D. Tanré, B. C. Gao, S. Platnick, S. A. Ackerman, L. A. Remer, R. Pincus, and P. A. Hubanks (2003), Cloud and aerosol properties, precipitable water, and profiles of temperature and humidity from MODIS, *IEEE Trans. Geosci. Remote Sens.*, *41*, 442–458.

Kistler, R., et al. (2001), The NCEP-NCAR 50-year reanalysis: Monthly means CD-ROM and documentation, *Bull. Am. Meteorol. Soc.*, *82*(2), 247–267.

Kushnir, Y., W. A. Robinson, P. Chang, and A. W. Robertson (2006), The physical basis for predicting Atlantic sector seasonal-to-interannual climate variability, *J. Clim.*, *19*, 5949–5970, doi:10.1175/JCLI3943.1.

Landsea, C. W., S. Feuer, A. Hagen, D. A. Glenn, J. Sims, R. Perez, M. Chenoweth, and N. Anderson (2012), A reanalysis of the 1921–1930 Atlantic hurricane database, *J. Clim.*, *25*, 865–885.

Liu, W. T., X. Xie, and K. B. Katsaros (2012), Observation of oceanic origin of Sahel precipitation from space, *Remote Sens. Environ.*, *123*, 593–599.

Ma, Y., and R. T. Pinker (2012), Shortwave radiative fluxes from satellites: An update, *J. Geophys. Res.*, *117*, D23202, doi:10.1029/2012JD018332.

Martonchik, J. V., D. J. Diner, R. Kahn, T. P. Ackerman, M. M. Verstraete, B. Pinty, and H. R. Gordon (1998), Techniques for the retrieval of aerosol properties over land and ocean using multi-angle imaging, *IEEE Trans. Geosci. Remote Sens.*, *36*(4), 1212– 1227.

McPhaden, M. J., et al. (1998), The Tropical Ocean-Global Atmosphere (TOGA) observing system: A decade of progress, *J. Geophys. Res.*, *103*, 14,169–14,240.

Mlawer, E. J., S. J. Taubman, P. D. Brown, M. J. Iacono, and S. A. Clough (1997), Radiative transfer for inhomogenous atmospheres: RRTM, a validated correlated-k model for the longwave, *J. Geophys. Res.*, *102*, 16,663–16,682.

Niu, X., R. T. Pinker, and M. F. Cronin (2010), Radiative fluxes at high latitudes, *Geophys. Res. Lett.*, *37*, L20811, doi:10.1029/2010GL044606.

Nussbaumer, E. A., and R. T. Pinker (2012), Estimating surface longwave radiative fluxes from satellites utilizing artificial neural networks, *J. Geophys. Res.*, *117*, D07209, doi:10.1029/2011JD017141.

Ohmura, A., et al. (1998), Baseline Surface Radiation Network (BSRN/WCRP): New precision radiometry for climate research, *Bull. Am. Meteorol. Soc.*, *79*, 2115–2136, doi:10.1175/1520-0477.

Oke, P., M. Martin, M. A. Balmaseda, G. Brassington, and K. Wilmer-Becker (2011), Report on the GODA Ocean View—CLIVAR GSOP Workshop on Observing System Evaluation and Intercomparison, Santa Cruz, Calif., 13–17 June. [Available at https://www.godae-oceanview.org/outreach/meetings-workshops/task-team-meetings/godae-oceanview-gsop-clivar-workshop/.]

Otterå, O. H., M. Bentsen, H. Drange, and L. Suo (2010), External forcing as a metronome for Atlantic multidecadal variability, *Nature Geosci.*, *3*, 688–694.

Pincus, R., S. Platnick, S. A. Ackerman, R. S. Hemler, and R. J. P. Hofmann (2012), Reconciling simulated and observed views of clouds: MODIS, ISCCP, and the limits of instrument simulators, *J. Clim.*, *25*(13), 4699–4720, doi:10.1175/JCLI-D-11–00267.1.

Pinker, R. T., H. Wang, and S. A. Grodsky (2009), How good are ocean buoy observations of radiative fluxes?, *Geophys. Res. Lett.*, *36*, L10811, doi:10.1029/2009GL037840.

Platnick, S., M. D. King, S. A. Ackerman, W. P. Menzel, B. A. Baum, J. C. Riédi, and R. A. Frey (2003), The MODIS cloud products: Algorithms and examples from Terra. *IEEE Trans. Geosci. Remote Sens.*, *41*, 459–473.

Reynolds, R. W., T. M. Smith, C. Liu, D. B. Chelton, K. S. Casey, and M. G. Schlax (2007), Daily high-resolution-blended analyses for sea surface temperature, *J. Clim.*, *20*, 5473–5496.

Rossow, W. B., and R. A. Schiffer (1999), Advances in understanding clouds from ISCCuP, *Bull. Am. Meteorol. Soc.*, *80*, 2261–2287.

Rossow, W. B., A. W. Walker, and L. C. Garder (1993), Comparison of ISCCP and other cloud amounts, *J. Clim.*, *6*, 2394–2418.

Ruiz-Barradas, A., J. A. Carton, and S. Nigam (2000), Structure of interannual-to-decadal climate variability in the Tropical Atlantic Sector, *J. Clim.*, *13*, 3285–3297, doi:10.1175/1520-0442(2000)013<3285:SOITDC>2.0.CO;2.

Santorelli, A., R. T. Pinker, A. Bentamy, K. B. Katsaros, W. M. Drennan, A. M. Mestas-Nuñez, and J. A. Carton (2011), Differences between two estimates of air-sea turbulent heat fluxes over the Atlantic Ocean, *J. Geophys. Res.*, *116*, C09028, doi:10.1029/2010JC006927.

Servain, J., A. J. Busalacchi, M. J. McPhaden, A. D. Moura, G. Reverdin, M. Vianna, and S. E. Zebiak (1998), A pilot research moored array in the tropical Atlantic (PIRATA), *Bull. Am. Meteorol. Soc.*, *79*(10), 2019–2031.

Shinoda, T., H. H. Hendon, and J. D. Glick (1998), Intraseasonal sea surface temperature variability in the tropical Pacific and Indian Oceans, *J. Clim.*, *11*, 1685–1702.

Simmons, A., S. Uppala, D. Dee, and S. Kobayash (2006), ERA-Interim: New ECMWF reanalysis products from 1989 onwards, *ECMWF Newsl.*, *110*, 26–35.

Smith, S., P. J. Hughes, and M. A. Bourassa (2010), A comparison of nine monthly air-sea flux products, *Int. J. Clim.*, *30*, 1002–1027, doi:10.1002/joc.2225.

Stubenrauch, C. J., et al. (2013), Assessment of global cloud datasets from satellites: Project and database initiated by the GEWEX radiation panel. *Bull. Am. Meteorol. Soc.*, *94*, 1031–1049.

Wang, C., D. B. Enfield, S.-K. Lee, and C. W. Landsea (2006), Influences of the Atlantic Warm Pool on Western Hemisphere summer rainfall and Atlantic hurricanes, *J. Clim.*, *19*, 3011–3028, doi:10.1175/JCLI3770.1.

Wang, H., and R. T. Pinker (2009), Shortwave radiative fluxes from MODIS: Model development and implementation, *J. Geophys. Res.*, *114*, D20201, doi:10.1029/2008JD010442.

Yu, L., X. Jin, and R. A. Weller (2008), Multidecade global flux datasets from the objectively analyzed air-sea fluxes (OAFlux) project: Latent and sensible heat fluxes, ocean evaporation, and related surface meteorological variables, *OAFlux Project Tech. Rep. OA-2008-01*, 64 pp., Woods Hole Oceanogr. Inst., Woods Hole, Mass.

Zhang Y. C., W. B. Rossow, A. A. Lacis, V. Oinas, and M. I. Mishchenko (2004), Calculation of radiative fluxes from the surface to top of atmosphere based on ISCCP and other global data sets: Refinements of the radiative transfer model and the input data, *J. Geophys. Res.*, *109*, D19105, doi:10.1029/2003JD004457.